Performance and characterization of a modular superconducting nanowire single photon detector system for space-to-Earth optical communications links

Brian E. Vyhnalek, Sarah A. Tedder, and Jennifer M. Nappier

National Aeronautics and Space Administration
Glenn Research Center
Cleveland, OH, USA

ABSTRACT

Space-to-ground photon-counting optical communication links supporting high data rates over large distances require enhanced ground receiver sensitivity in order to reduce the mass and power burden on the spacecraft transmitter. Superconducting nanowire single-photon detectors (SNSPDs) have been demonstrated to offer superior performance in detection efficiency, timing resolution, and count rates over semiconductor photodetectors, and are a suitable technology for high photon efficiency links. Recently photon detectors based on superconducting nanowires have become commercially available, and we have assessed the characteristics and performance of one such commercial system as a candidate for potential utilization in ground receiver designs. The SNSPD system features independent channels which can be added modularly. We analyze the scalability of the system to support different data rates, as well as consider coupling concepts and issues as the number of channels increases.

Keywords: Optical communications, single photon detectors, superconducting nanowire

1. INTRODUCTION

Free-space optical communications (FSOC) is an extremely promising solution for higher-rate data communications from lunar and inter-planetary distances to Earth-based ground stations, offering many advantages as compared to radio-frequency (RF) technologies such as the potential for substantially higher data rates and lower mass, power and size. NASA's 2013 Lunar Laser Communication Demonstration (LLCD) showed that FSOC from the Moon to Earth is feasible and advantageous by achieving up to 622 Mbps on the optical downlink, substantially exceeding the fastest Ka-band RF links.[1] With NASA's ongoing efforts such as the Jet Propulsion Laboratory's (JPL) Deep Space Optical Communications (DSOC) project,[2] the Laser Communication Relay Demonstration (LCRD),[3] and the Optical-to-Orion (O2O) project, the future prospects continue to improve for mission-operational free-space optical communications.

A number of enabling technologies were demonstrated in the LLCD mission including the use of multi-element niobium nitride (NbN) and multi-element tungsten silicide (WSi) superconducting nanowire single-photon detector (SNSPD) arrays developed by the Massachusetts Institute of Technology's Lincoln Laboratory and JPL, respectively, and used at the LLCD ground stations in White Sands, New Mexico and on top of Table Mountain in California.[1] SNSPDs have been under investigation since the early 2000s,[4] and have shown great promise for a variety of ultra-sensitive light detection applications - in particular for applications at telecommunications wavelengths near 1550 nm where they substantially outperform single-photon InGaAs avalanche photo-diodes (APDs) and photomultiplier tubes (PMTs).[5–7] Until very recently photon detectors based on SNSPDs were not commercially available, thus limiting widespread usage. With several commercial vendors offering turnkey multi-channel SNSPD systems with simplified cryogenics, SNSPDs are increasingly viable as an operational component for space-to-ground high-photon efficiency FSOC links.

Send correspondence to brian.e.vyhnalek@nasa.gov

2. DETECTOR SYSTEM CHARACTERIZATION

We characterized a two-detector Opus One™ system (Figure 1) from Quantum Opus, LLC which operates at a temperature of 2.5 K using a closed-cycle helium water-cooled cryocooler housed in a 3U 19-inch rack-mountable unit, and is modularly exapandable to up to 16 detectors onto a single cold head. The nanowire detectors are optimized for 1550 nm operating wavelength, self-aligned for maximum coupling efficiency,[8,9] and coupled to single-mode fiber inputs. Electrically the devices are current biased with adjustable front panel controls, and coupled to 50 Ω coaxial readout cables to room temperature amplifiers with 500 MHz bandwidth and a maximum 55.6 dB gain.[10] The system is powered via a Standford Research Systems SIM900 mainframe, and can be computer controlled either serially or through GPIB interface.

Figure 1: Opus One™ SNSPD system.

The system detection efficiency (SDE) and dead-time characterization was measured using the setup shown in Figure 2. A benchtop continuous wave (CW) distributed feedback (DFB) laser source was thermally controlled to output precisely at an operating wavelength of 1550 nm, and attenuated to a mean photon number of ≈ 168,000 photons/s using both fixed and variable attenuators. Each component in the setup was separately characterized

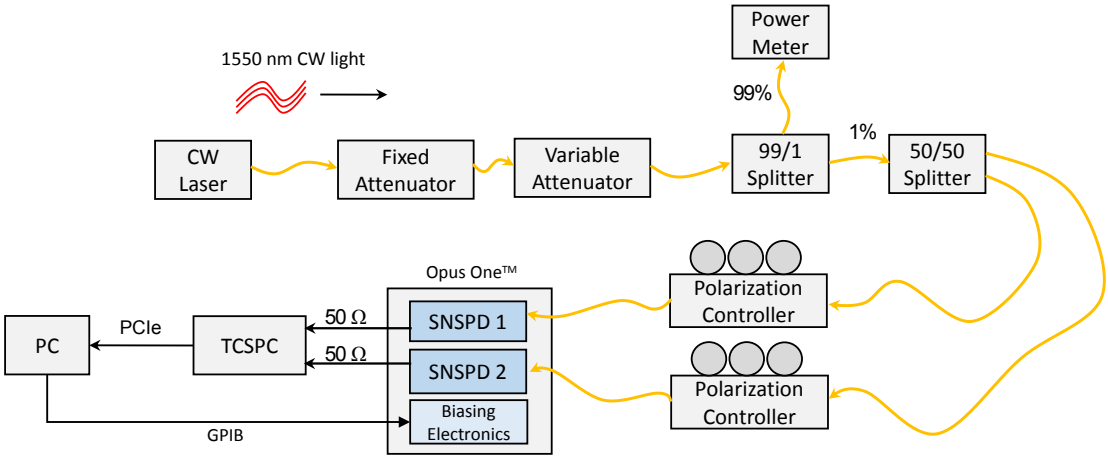

Figure 2: Characterization setup diagram

with a calibrated 1550 nm InGaAs power meter with 0.1 pW resolution to determine fiber loss, fiber splitting ratios, and attenuation factors before being assembled together with a tap to the power meter to monitor input power. Fiber paddle polarization controllers were placed before the inputs to the fiber coupling to the SNSPDs to adjust the input state of polarization in order to accommodate the polarization sensitivity of the detectors. The ouput pulses from the SNSPDs were sent to a multi-channel time-correlated single-photon counting (TCSPC) card, capable of 25 ps resolution and up to 50 Mcps continuous counting per channel.

Dark count rate and background counts were initially determined for each detector channel as a function of bias current as shown in Figure 3a, where each data point is the average of 10 measurements. The dark count rates were measured with input fibers to the system disconnected and the inputs to the detectors capped, whereas the background count rates were determined with the input fibers connected, but with the laser blocked by a shutter. Each channel displayed about the same level of dark count rate, less than 10 - 30 cps for bias currents $I_B < 15$ μA, and less than 100 cps for $15 < I_B \lesssim 15.5$ μA before increasing by several orders of magnitude between 15 and $I_{SW} \approx 16$ μA, the level of input current at which the devices switch from the superconducting to the normal state. Background count rates were nearly constant and identical for both channels at a level of about 6 kcps, almost entirely due to room-temperature blackbody radiation except for at bias levels approaching I_{SW} in which dark counts increase significantly.

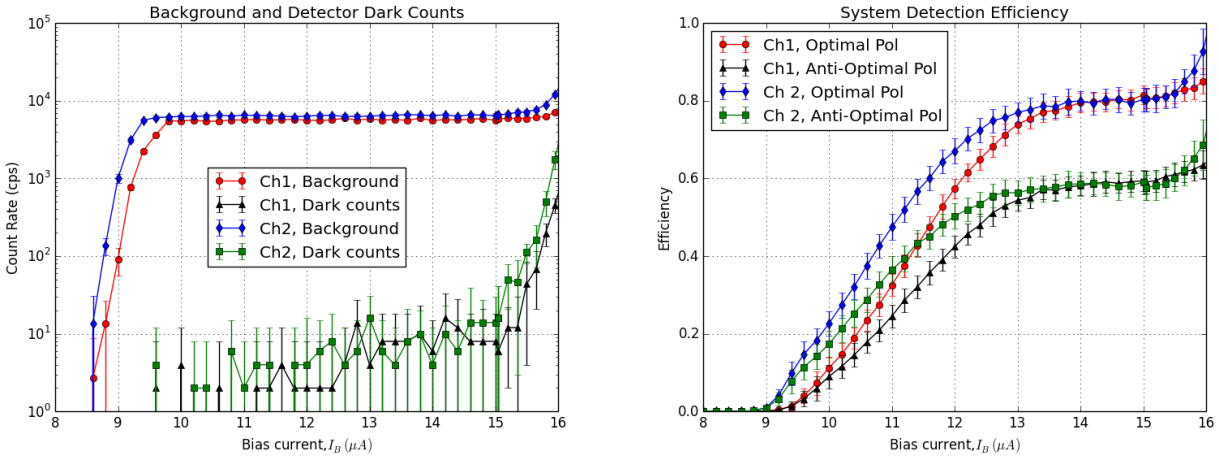

(a) (b)

Figure 3: Background count rate and system detection efficiency vs. bias current.

System detection efficiency (SDE) was estimated for each channel for both optimal and anti-optimal input polarizations. Figure 3b shows the average and one standard deviation of 10 measurements for each bias current. The system detection efficiency was determined by $SDE = (R_{out} - BCR)/R_{in}$, where R_{out} is the measured output count rate, BCR is the background count rate measured previously, and R_{in} is the input photon flux estimated from power meter measurements and accounting for system losses. For both channels the SDE for optimal input polarization (SDE_{max}) reached a plateau value of $80 \pm 2.8\%$ for bias currents of $\approx$ 13.5 - 15.5 μA ($0.84I_{SW}$ - $0.97I_{SW}$) and a maximum value of $82 \pm 2.8\%$ for channel 1 and $82 \pm 3.1\%$ for channel 2 at $I_B = 0.97I_{SW}$, after which dark counts increase significantly above 100 cps. With the polarization controllers adjusted such that the input state of polarization was orthogonal to the optimal state, a plateau value of $\approx 60 \pm 3.0\%$ (SDE_{min}) for the same bias current range, and a maximum value of $61.0 \pm 3.0\%$ for channel 1 and $60.2 \pm 2.9\%$ for channel 2 at $I_B = 0.97I_{SW}$. The polarization dependence ratio, $r_{pol} = SDE_{max}/SDE_{max}$, is determined to be a factor of $\approx$ 1.25 dB.

A typical output pulse is shown in Figure 4a, at a bias level of $I_B \approx 15$ μA. The pulse height is 588 mV, but can range between $\approx$ 300 mV - 600 mV depending on I_B. Rise time is 1 ns, and the 90% - 10% fall time of the pulse is 35 ns, while the $1/e$ fall time is $\tau_r \approx 16$ ns, faster than the values reported for WSi or molybdenum silicide (MoSi) SNSPDs[11,12] but slower than values reported for Nb and NbN devices.[4–6,13] Figure 4b shows the histogram of the time interval for subsequent pulses, peaking at 22.5 ns, and with no counts registered for interarrival times less than 12 ns. The count rate as a function of the input photon flux is shown in Figure 5 with a linear fit to the first 6 data points, and a Monte Carlo simulation curve based on a phenomenological exponential recovery model of detection efficiency, i.e.

$$SDE(t) = SDE_{max}\left(1 - e^{-(t-t_0)/\tau_r}\right), \tag{1}$$

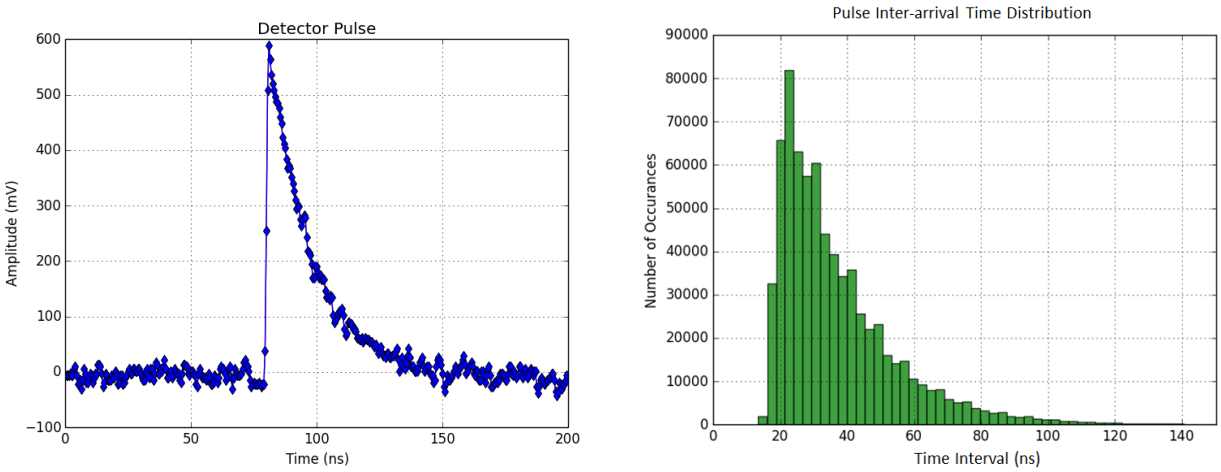

(a) (b)

Figure 4: Example output pulse and inter-arrival time histogram.

where SDE_{max} is the maximum system detection efficiency, i.e. 82%, τ_r is the $1/e$ pulse decay time, and t_0 is a Poisson-distributed photon arrival time. From Figure 5 it can be seen that the measured counts/s increase linearly until about 12 Mcps afterwhich begin to plateau approaching a maximum of $\approx$ 48 Mcps, although at severly degraded detection levels approaching 4% efficiency.

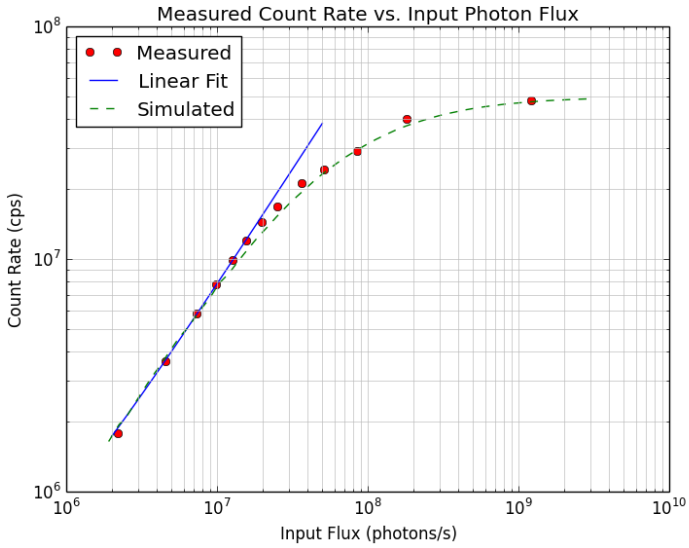

Figure 5: Measured count rate vs. estimated input photon flux for one detector.

To characterize the system instrument response function (IRF) and detection jitter, the setup was modified as shown in Figure 6 to include a 1550 nm femtosecond fiber laser in place of the CW DFB laser. The femtosecond laser output pulses with a minimum of 100 fs FWHM, and was attenuated to a level of $\ll 1$ photon/pulse. An electrical pulse was also simultaneously output from the laser synchronized with the rising edge of the optical pulse, and was fed into the synchronization input of the TCSPC card. The TCSPC card then measured the time interval between the rising edge of the electrical sync pulse from the laser and the rising edge of the output

pulse from the SNSPDs, and built up a statistical distribution with 25 ps bins. Figure 7 shows measured IRFs for channel 1 at different bias currents.

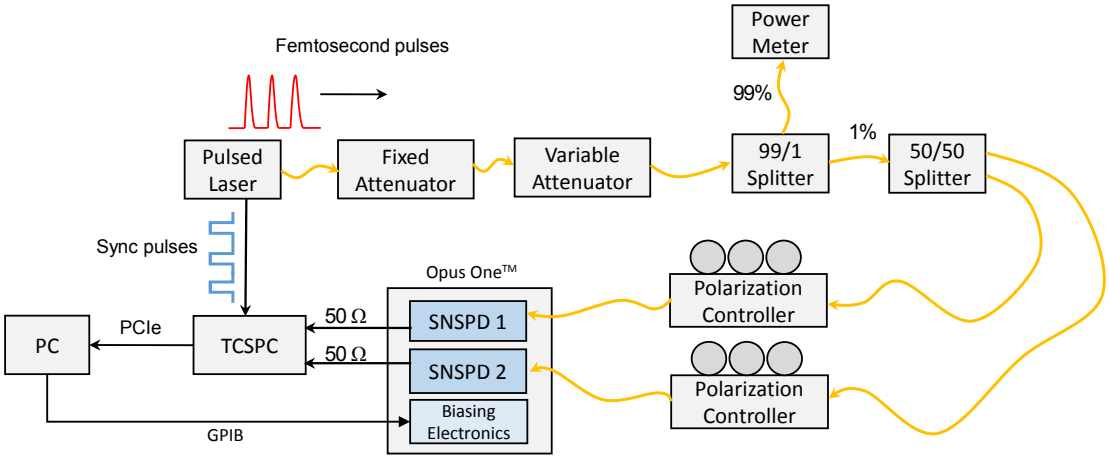

Figure 6: IRF/jitter characterization setup diagram.

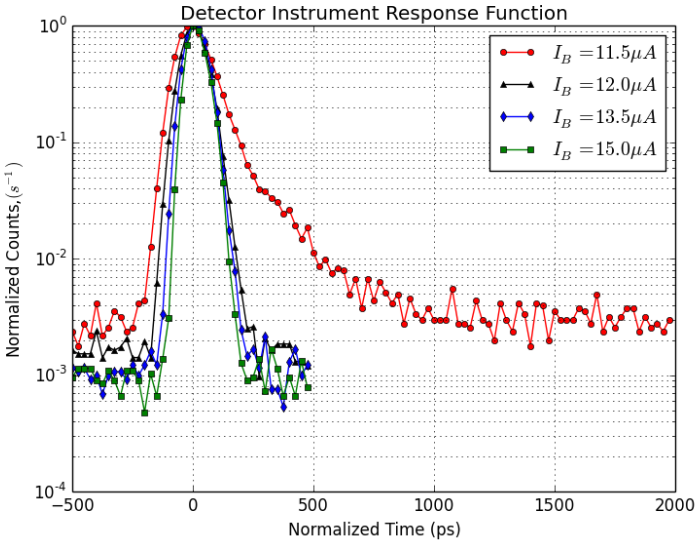

Figure 7: Example measured instrument response functions.

For each of the measured IRFs we fit a Gaussian function as shown in Figure 8a, and from the fitted functions extracted the total measurement jitter, defined as the FWHM of the IRF.[12] However, these values also include jitter effects from the input laser, input sync pulse, and TCSPC card, thus the system jitter J_S can be determined from[12]

$$J_{meas}^2 = J_{laser}^2 + J_{sync}^2 + J_{TCSPC}^2 + J_S^2. \tag{2}$$

With $J_{laser} = 0.06$ ps, $J_{sync} = 4.0$ ps, and $J_{TCSPC} = 20.0$ ps, J_S was calculated for each channel, and the dependence on bias current I_B is shown in Figure 8b. From Figure 7 it can be seen that the width of the IRF decreases with increasing I_B, and similarly Figure 8b shows that J_S decreases from $\approx$ 110 ps - 120 ps at $I_B = 0.75I_{SW}$ to $\approx$ 80 - 85 ps at $I_B = 0.97I_{SW}$. The fact that the system jitter decreases with increasing I_B is consistent with the fact that at higher I_B the output pulse amplitudes are larger, and therefore higher signal-to-noise ratio.[11]

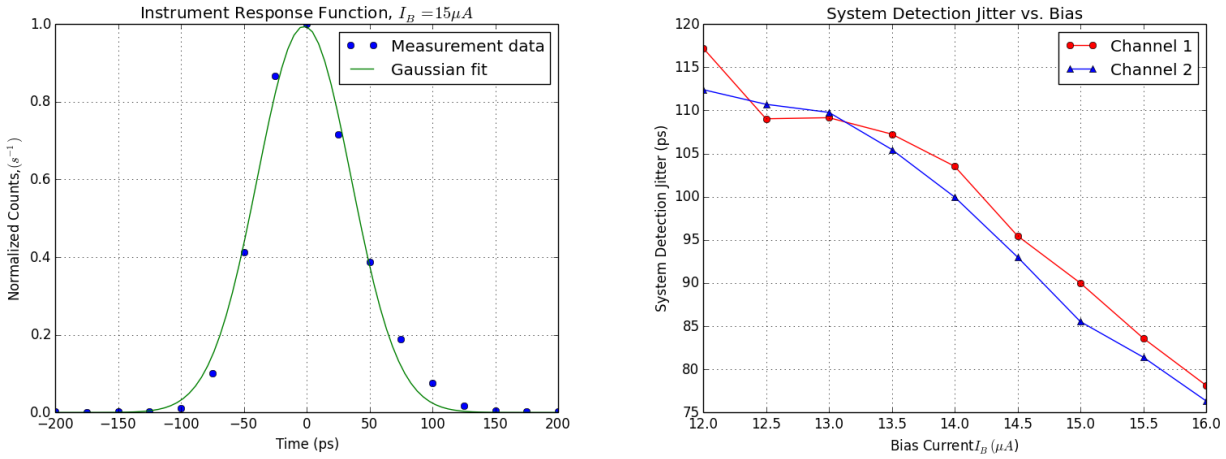

(a) (b)

Figure 8: Example IRF with Gaussian fit and system jitter vs. bias current I_B.

3. DEMONSTRATION IN AN OPTICAL COMMUNICATIONS LINK

To demonstrate the utility of the commercial off-the-shelf (COTS) SNSPD system in a communications link, we perform optical link testing with the setup shown in Figure 9. The additions from the characterization setup were a polarization-adjustable 1550 nm CW laser source with a polarization extinction ratio of up to 40 dB, a high extinction-ratio $LiNbO_3$ electro-optic modulator capable of over 50 dB of intensity extinction, and a fiber-coupled tungsten-halogen broadband light source with a 1550 ± 20 nm bandpass filter along with an additional variable attenuator to control input background noise levels. The input to the modulator was

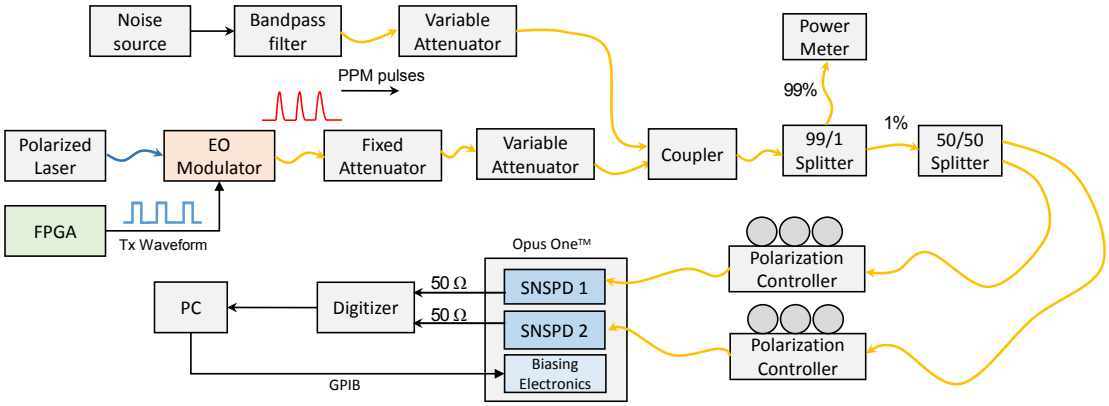

Figure 9: Laboratory test setup for optical link testing.

a serially-concatenated pulse-position modulated (SCPPM)[14] signal generated from a field programmable gate array (FPGA) with selectable code rates $r = \{1/3, 1/2, 2/3\}$, PPM orders $M = \{4, 8, 16, 32, 64, 128, 256\}$, and adjustable slot width T_s, consistent with the Consultative Committee for Space Data Systems (CCSDS) optical communications high photon efficiency (HPE) downlink transmit waveform modes.[15,16] For the purposes of the demonstration we selected $M = 32$, with 8 guard slots, $r = 1/3$, and $T_s = 4$ and 2 ns, corresponding to data rates of 10 and 20 Mbps respectively. Additionally, the noise source attenuation level was set such as to consistently produce an average detected background count rate of $K_b \approx 0.01$ counts per slot. Both the modulated 1550 nm optical signal and the filtered broadband noise source were combined before being input to the SNSPD detectors, and the output signals were sampled with a high-speed digitizer at a rate of 1 GS/s before being post processed.

4. RESULTS

The optical link was successfully closed error-free (zero bit errors) at both the 10 Mbps and 20 Mbps rates using the output from only a single detector, with a predicted average number of detected signal counts per PPM symbol of $K_s \approx 0.8$. Combining the two channels together resulted in nearly double detected signal counts per PPM symbol as anticipated. Based on these results and simulation results such as those shown in Figures 10a and 10b, we expect that 40 Mbps rates ($T_s = 1$ ns) are possible with a single detector in low background conditions, and that 80 Mbps ($T_s = 0.5$ ns) data rates are achievable using at least 2 detectors combined. These simulations

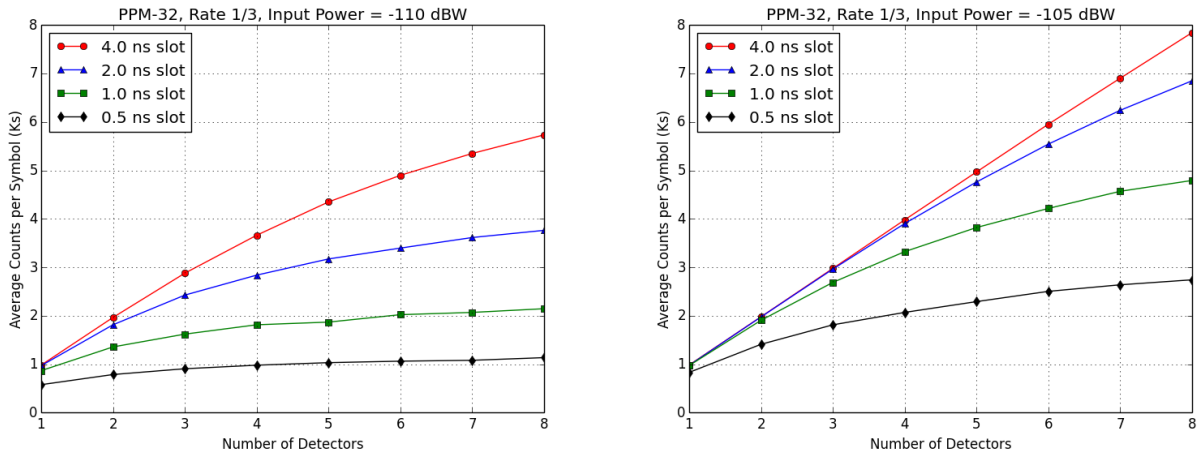

(a) (b)

Figure 10: Simulated average number of detected signal counts per PPM symbol vs. number of detectors for PPM-32 rate 1/3 with 8 guard slots, for fixed signal and background photon flux.

were performed using the measured detector efficiency and dead time parameters, and by assigning a randomly generated Poisson-distributed photon number and arrival times within either a PPM signal slot or a background slot. The average photon number per slot was determined from the average input signal and background optical power, which for Figures 10a and 10b were -110.0, -121.2 dBW and -105.0, -121.2 dBW respectively. In this case, the background power level of -121.2 dBW was selected to produce an average background level of $K_b \approx 0.01$ counts per slot. A photon was considered to be detected if a uniformly-distributed random number over the interval [0,1] was less then the SDE at a photon arrival time t, and detector blocking effects were accounted for by allowing the detector $SDE(t)$ to follow the exponential recovery model of Eq. 1. Each successful photon detection was then registered as a signal count if the arrival/detection time was within a signal slot, otherwise as a background count.

The required number of detectors for a target data rate is a multidimensional problem depending on the modulation order, code rate, background power and expected signal power. However, because detectors plus associated control and amplifier electronics can be added modularly with minimal downtime, an SNSPD system such as this could support a variety of different optical communications links requiring single-photon sensitivity. The modular structure appropriately lends itself to receiver array architectures, but also for single aperture receivers as well. In this case losses from splitting in order to couple to multiple detectors will have to be carefully considered, and more efficient low-loss interfaces such as photonic lanterns[17] may need to be further developed.

5. CONCLUSION

We characterized a COTS superconductor nanowire single-photon detector system to assess parameters such as detection efficiency, dark count rate, reset time, maximum count rate, and timing jitter to determine suitability

of the current state of such systems to support upcoming and future space-to-ground missions requiring single-photon sensitivity. The measured SNSPD parameters were similar to the results reported for WSi[12] and MoSi[11] in terms of detection efficiency and detection jitter, and exceeded the results reported for count rate and reset time for single-element devices in those materials. We successfully closed an optical communications link with zero bit errors, and have shown that an error-free 20 Mbps data rate is possible with a single detector while anticipating that 80 Mbps may be possible with two detectors. As SNSPD technology continues to mature continual improvements in sensitivity, reset time and jitter are anticipated. Along with the ability to add detectors modularly in parallel, thereby adding a degree of flexibility to system design, the prospects for optical communications used operationally in lunar and inter-planetary space missions continue to improve.

ACKNOWLEDGMENTS

The authors would like to acknowledge the support by the NASA Space Communications and Navigation (SCaN) funded Integrated Radio and Optical Communications (iROC) project, and Aaron Miller and Tim Rambo from Quantum Opus LLC for useful discussions.

REFERENCES

1. B. S. Robinson, D. M. Boroson, D. A. Burianek, D. V. Murphy, F. I. Khatri, J. W. Burnside, J. E. Kansky, A. Biswas, Z. Sodnik, and D. M. Cornwell, "The NASA Lunar Laser Communication Demonstration - successful high-rate laser communications to and from the Moon," in *Proceedings of SpaceOps*, 2014.
2. H. Hemmati, A. Biswas, and I. Djordevic, "Deep Space Optical Communications: Future perspectives and applications," in *Proceedings of the IEEE*, **99**(11), pp. 2020 – 2039, 2011.
3. B. L. Edwards, D. Israel, K. Wilson, J. Moores, and A. Fletcher, "Overview of the laser communications relay demonstration project," in *Proceedings of SpaceOps*, pp. 11 – 15, 2012.
4. R. Sobolewski, A. Verevkin, G. N. Gol'tsman, A. Lipatov, and K. Wilsher, "Ultrafast superconducting single-photon optical detectors and their applications," *IEEE Transactions on Applied Superconductivity* **13**, pp. 1151–1157, June 2003.
5. A. J. Kerman, E. A. Dauler, B. S. Robinson, R. Barron, D. O. Caplan, M. L. Stevens, J. J. Carney, S. A. Hamilton, W. E. Keicher, J. K. W. Yang, K. Rosfjord, V. Anant, and K. K. Berggren, "Superconducting nanowire photon-counting detectors for optical communications," *Lincoln Laboratory Journal* **16**(1), pp. 217–224, 2006.
6. C. M. Natarajan, M. G. Tanner, and R. H. Hadfield, "Superconducting nanowire single-photon detectors physics and applications," *Superconductor Science and Technology* **25**(6), 2012.
7. R. Hadfield, "Single-photon detectors for optical quantum information applications," *Nature Photonics* **3**, Dec. 2009.
8. Quantum Opus, *Nanowire Datasheet*, Jan. 2017.
9. A. J. Miller, A. E. Lita, B. Calkins, I. Vayshenker, S. M. Gruber, and S. W. Nam, "Compact cryogenic self-aligning fiber-to-detector coupling with losses below one percent," *Optics Express* **19**, pp. 9102 – 9110, May 2011.
10. Quantum Opus, *Nanowire Bias and Readout Electronics Datasheet*, Jan. 2017.
11. V. B. Verma, B. Korzh, F. Bussières, R. D. Horansky, S. Dyer, A. Lita, L. Vayshenker, F. Marsili, M. D. Shaw, H. Zbinden, R. P. Mirin, and S. W. Nam, "High-efficiency superconducting nanowire single-photon detectors fabricated from MoSi thin-films," *Optics Express* **23**, Dec. 2015.
12. F. Marsili, V. B. Verma, J. A. Stern, S. Harrington, A. E. Lita, T. Gerrits, I. Vayshenker, B. Baek, M. D. Shaw, R. P. Mirin, and S. W. Nam, "Detecting single infrared photons with 93% system efficiency," *Nature Photonics* **7**, pp. 210 – 214, 2013.
13. S. Miki, M. Fujiwara, M. Sasaki, B. Baek, A. J. Miller, R. H. Hadfield, S. W. Nam, and Z. Weng, "Large sensitive-area NbN nanowire superconducting single-photon detectors fabricated on single-crystal MgO substrates," *Applied Physics Letters* **92**, 2008.
14. B. Moison and J. Hamkins, "Coded modulation for the deep-space optical channel: Serially concatenated pulse position modulation," *The Interplanetary Network Progress Report* **42**(161), 2005.

15. J. M. Nappier and N. Lantz, "Development of an optical slice for an RF and optical software defined radio," in *Proc. SPIE 10524 - Free-Space Laser Communication and Atmospheric Propagation XXX*, 2018.
16. Consultative Committee for Space Data Systems (CCSDS), *High Photon Efficiency Optical Communications: Coding & Synchronization, Proposed Recommended Standard*, Sep 2016.
17. T. A. Birks, I. Gris-Sánchez, S. Yerolatsitis, S. G. Leon-Saval, and R. R. Thomson, "The photonic lantern," *Advances in Optics and Photonics* **7**, pp. 107 – 167, 2015.